atmosphere

MDPI

Article

Satellite Radiance Data Assimilation Using the WRF-3DVAR System for Tropical Storm Dianmu (2021) Forecasts

Thippawan Thodsan [1], Falin Wu [1,*], Kritanai Torsri [2], Efren Martin Alban Cuestas [3] and Gongliu Yang [1]

[1] SARS Laboratory, School of Instrumentation and Optoelectronic Engineering, Beihang University, Beijing 100191, China; thippawan@hii.or.th (T.T.); yanggongliu@buaa.edu.cn (G.Y.)
[2] Hydro-Informatics Institute, Ministry of Higher Education, Science, Research and Innovation, Bangkok 10900, Thailand; kritanai@hii.or.th
[3] Asian Institute of Technical Sciences, Bangkok 10400, Thailand; martinalban@aitsworld.com
* Correspondence: falin.wu@buaa.edu.cn

Abstract: This study investigated the impact of the assimilation of satellite radiance observations in a three-dimensional variational data assimilation system (3DVAR) that could improve the tracking and intensity forecasts of the Tropical Storm Dianmu in 2021, which occurred over parts of southeast mainland Asia. The weather research and forecasting (WRF) model was used to conduct the assimilation experiments of the storm. Four sets of numerical experiments were performed using the WRF. In the first, the control experiment, only conventional data in Binary Universal Form for the Representation of Meteorological Data (PREPBUFR) observations from the National Centers for Environmental Prediction (NCEP) were assimilated. The second experiment (RDA1) was performed with PREPBUFR observations and satellite radiance data from the Advanced Microwave Unit-A (AMSU-A), and the Advanced Technology Microwave Sounder (ATMS). PREPBUFR observations and the High-resolution Infrared Radiation Sounder (HIRS-4) were used in the third experiment (RDA2). The fourth experiment (ALL-OBS) used the assimilation of PREPBUFR observations and all satellite radiance data (AMSU-A, ATMS, and HIRS-4). The community radiative transfer model was used on the forward operator for the satellite radiance assimilation, along with quality control and bias correction procedures, before assimilating the radiance data. To evaluate the impact of the assimilation experiments, a forecast starting on 00 UTC 23 September 2021, was produced for 72 h. The results showed that the ALL-OBS experiment improved the short-term forecast up to ~24 h lead time, as compared to the assimilation considering only PREPBUFR observations. When all observations were assimilated into the model, the storm's landfall position, intensity, and structure were accurately predicted. In the deterministic forecast, the tracking errors of the ALL-OBS experiment was consistently less than 40 km within 24 h. The case study of Tropical Storm Dianmu exhibited the significant positive impact of all observations in the numerical model, which could improve updates for initial conditions and storm forecasting.

Keywords: variational data assimilation; satellite radiance data; tropical storm; weather research and forecasting (WRF) model

Citation: Thodsan, T.; Wu, F.; Torsri, K.; Cuestas, E.M.A.; Yang, G. Satellite Radiance Data Assimilation Using the WRF-3DVAR System for Tropical Storm Dianmu (2021) Forecasts. *Atmosphere* **2022**, *13*, 956. https://doi.org/10.3390/atmos13060956

Academic Editors: Zhibin Sun, Yan-An Liu and Zigang Wei

Received: 15 April 2022
Accepted: 10 June 2022
Published: 12 June 2022

1. Introduction

Tropical cyclones (TCs) are known to cause damage and lead to great losses in terms of property and economy, which is a major concern that drives the challenge to improve cyclone forecasting [1,2]. Tropical storms form over warm oceanic regions when atmospheric and oceanic conditions are favorable [3], such as tropical ocean regions with latitudes greater than 5°, sea surface temperatures (SSTs) greater than 26.5 °C, and limited vertical wind shear to facilitate thunderstorm development [4]. Tropical storms develop more frequently in the South China Sea than in the Indian Ocean. The highest rates of cyclonic disturbance start in September and move from the east to the northeast of Thailand, which

is known to be highly vulnerable to damage by tropical storms on its vast agricultural and developmental activities.

An accurate forecast of the movement, intensity, and location of land-falling tropical storms is essential for warning and planning for disaster mitigation. The numerical weather prediction (NWP) model has been improved so that it can be used for predicting tropical cyclones. This improvement includes the data assimilation of increased satellite observations for short-term weather forecasts, which have been recognized to precisely define the initial conditions in the NWP model [5,6]. Both tropical cyclone tracking and intensity forecasting have been improved by previous data assimilation studies. For instance, Kattamanchi et al. [7] predicted six TCs (Vardah, Gaja, Phethai, Mora, Fani, and Amphan) using a 3DVAR method for assimilation. They concluded that the assimilation of surface winds with the WRF model was effective for both tracking and intensity predictions. They also reported that the assimilation of Scatterometer SATellite-1 (SCATSAT-1) data surface winds improved cyclone tracking and intensity predictions. Xu et al. [8] used weather research and forecasting data assimilation (WRFDA) to assess the impact of the assimilation of infrared atmospheric sounding interferometer (IASI) radiance measurements on Hurricane Maira (2011) and Typhoon Megi (2010) forecasts. A cloud-detection scheme implemented in WRFDA was used to identify cloud contamination in radiance measurements from high-spectral-resolution infrared sounders. The IASI radiance assimilation was found to improve the depiction of dynamic and thermodynamic vortex formations in the storm. The assimilation of microwave humidity sounder (MHS) radiance data from the FY-3B satellite was studied in a recent study by Xu et al. [9] in the assessment and prediction of binary typhoons Linfa and Chan-hom in the Pacific during 2015. The study emphasized the robustness of the results using FY-3B satellite humidity sounder (MHS) radiance data assimilation and the regional WRF model and its data assimilation systems, using a hybrid 3DVAR on the binary interaction of the typhoons and the reliability of the results. Moradi et al. [10] described and illustrated an enhanced Bayesian Monte Carlo integration (BMCI) retrieval method in a data assimilation system. Using data from an advanced technology microwave sounder (ATMS) and a Global Precipitation Measurement (GPM) microwave imager, this study found that the assimilation of BMCI retrievals could affect a cyclone of dynamical properties, such as a stronger warm core, a symmetric eye, and vertical wind.

Furthermore, studies have shown that microwave radiance data and infrared sounders have more information in vertical profile of sounding observations and the inner structure of the storm. A study by Deb et al. [11] demonstrated that assimilating the INSAT-3D atmospheric wind vectors into the WRF model improved cyclonic storm-tracking forecast errors. Singh et al. [12] revealed that the assimilation of both NCEP PREPBUFR and radiance data could capture the structure of the storm and reduce tracking errors for different lead-time forecasts, which caused the improvement of the initial conditions for the storm. Lindskog et al. [13] used a large number of observations from traditional observations, radars, scatterometer data, and satellite radiances to produce initial states using 3DVAR and found that the assimilation of microwave humidity sounder 2 (MWHS2) and the Advanced Microwave Sounding (AMSU-A) radiances was beneficial in reducing systematic observation errors and excluding gross errors. The impacts of the assimilation of FY-3D MWHS2 radiance data under clear skies for Tropical Storm Ampil were studied by Xu et al. [14]. The study used data from an experiment assimilating both the Global Telecommunications System (GTS) and FY-3D MWHS2 radiance data, and a comparison experiment using only GTS data was also conducted. Thodsan et al. [15] evaluated the impact of the assimilation of multiplatform observations on forecasts of heavy rainfall events in Thailand using a 3DVAR assimilation method. According to their study, they reported that the assimilation experiments performed using multiplatform observations had better results than those using only local observations. These studies have reported improvements in forecast tracking errors and the position of rainfall prediction in short-term forecasts. Additional assimilations of satellite data and multiplatform observations in numerical weather prediction can be found in [5,7,16–22], among others.

During the 2021 monsoon season, Tropical Storm Dianmu's landfall affected parts of mainland Southeast Asia, which included Vietnam, Laos, and Thailand. It was reported as the most damaging storm of the 2021 monsoon season. This particular tropical storm was of interest in this study. The objective of the present study is to evaluate the impact of the assimilation of radiance data from various satellite instruments on the forecasts of Tropical Storm Dianmu using a 3DVAR assimilation method. Vertical information is abundant due to the coarser horizontal resolution of the Global Forecasting System (GFS) analysis data. Therefore, we expected that the assimilation of available satellite radiance data can improve forecasts of the initial conditions, as well as of the storm. The remaining parts of this paper are arranged as follows: A brief description of Tropical Storm Dianmu is presented in Section 2. The methodology of the forecast model, the experimental setup, the data used, and the 3DVAR assimilation method are presented in Section 3. The results of the numerical experiments and the discussion are given in Section 4. Finally, a conclusion is provided in Section 5.

2. Brief Description of Tropical Storm Dianmu, 2021

Tropical Storm Dianmu was a tropical cyclone that originated in the South China Sea in September 2021. The storm gradually intensified into a tropical storm at 00 UTC on 22 September 2021 and translated from a west to a north-west direction, gradually intensifying into a tropical storm at 06 UTC on 23 September 2021, with a maximum speed of 18 m/s and a minimum pressure of 1000 hPa, the storm reached its peak intensity. The storm crossed central Vietnam and southern Laos at 12 UTC the same day and weakened to a low-pressure area three hours later. It dissipated over Northeastern Thailand at 12 UTC on 24 September.

The best tracking data of the Japan Meteorological Agency (JMA) for Tropical Storm Dianmu is presented in Figure 1. The storm has caused widespread rainfall with heavy to very heavy rainfall over the central district of Vietnam, several provinces in Southern Laos, and Northeastern Thailand. There were eight reported deaths as a consequence of Tropical Storm Dianmu and resulting floods in Thailand and Vietnam, with another loss of 5 people and huge crop losses attributed as well [23]. The storm affected over 73,000 households, and the heavy rainfall caused floods in these countries. The significant feature of the system was that it extended its movement for 12 h close to the coast, resulting in unusually heavy rainfall.

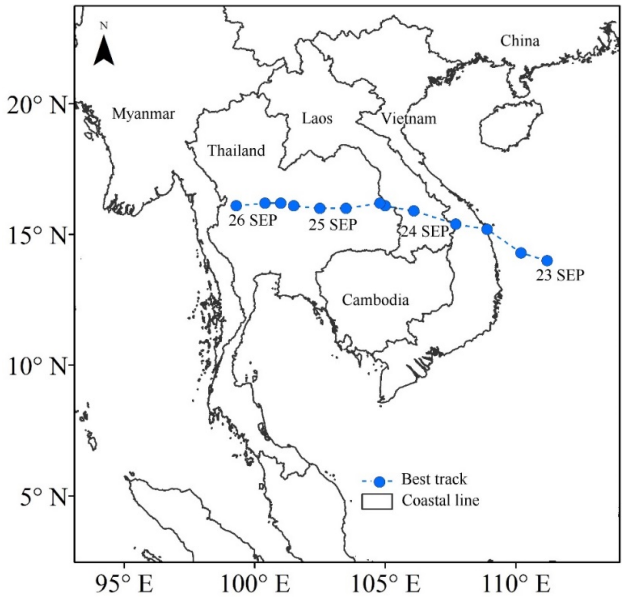

Figure 1. Observed tracking data from JMA during 00 UTC on 23 September to 00 UTC on 26 September 2021 for Tropical Storm Dianmu.

3. Methodology and Data

3.1. Forecast Model

The WRF variational Data Assimilation (version 3.9.1) forecast model was used in this study due to its higher-order mass conservation characteristics and advanced physics. Three-dimensional winds, potential temperatures, geopotential, surface pressure, turbulent kinetic energy, and scalar were among the prognostic variables in the model, which was made up of fully compressible nonhydrostatic equations. Figure 2 shows the model configuration. The outer domain (d01) covered 226 × 196 grid points with a 27 km horizontal resolution, and the inner domain (d02) has 430 × 340 grid points with a 9 km horizontal resolution and with 31 vertical levels. The physics options included Eta microphysics [24], the Yonsei University (YSU) boundary layer scheme [25], the rapid radiative transfer model (RRTM) long-wave radiation scheme [26], the Dudhia scheme for short-wave radiation [27], the Noah land surface model, and the Betts–Miller–Janjic (BMJ) cumulus parameterization scheme [28].

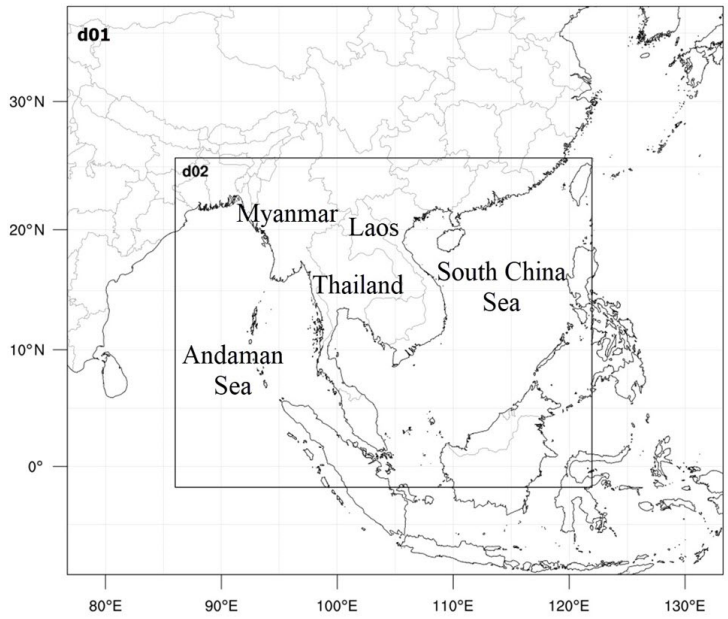

Figure 2. Model domains used for the 3DVAR assimilation method in this study.

3.2. Experimental Setup

Four experiments were carried out with data assimilation for the Dianmu storm in late September 2021. The first experiment was the control experiment (CNTL), with the assimilation of NCEP PREPBUFR observations (such as data from land and upper-air radiosondes, oceanic surface winds, and atmospheric wind), whose datasets were assimilated for the control (CNTL) experiment. The second experiment, hereafter referred to RDA1, used AMSU-A and ATMS radiance data and the available NCEP PREPBUFR observations. The third experiment, RDA2, used the High-resolution Infrared Radiation Sounder (HIRS-4) radiance data and the available NCEP PREPBUFR observations, as shown in Table 1. Finally, in the fourth experiment, ALL-OBS, the TC was initialized by assimilating the AMSU-A, ATMS, and HIRS-4 radiance data and all the available NCEP PREPBUFR observations. Descriptions of the data type, the platform, and the parameters used to assimilate into the WRF model are summarized in Table 1 and the experiment designs for the study are summarized in Table 2. Note that all the assimilation experiments, the model was initialized at 00 UTC 23 September 2021.

Table 1. Datasets assimilated for the CNTL experiment.

Observation	Platform	Assimilation Parameters
Upper air	PILOT, SOUND	u, v, t, q
Land surface	SYNOP, METAR	u, v, t, p, q
Marine surface	SHIP	u, v, t, p, q
Satellite	GEOAMV, QuikSCAT	u, v

Table 2. Design of the experimental setup.

Name of the Experimental Setup	Data Used in the Assimilation
CNTL	Mentioned in Table 1
RDA1	CNTL + AMSU-A+ATMS
RDA2	CNTL + HIRS-4
ALL-OBS	CNTL + AMSU-A+ATMS+HIRS-4

3.3. Data Used

The initial conditions for the numerical experiments were derived from the NCEP GFS analysis at 0.5° × 0.5° horizontal resolutions. The model integration of time-varying lateral boundary conditions was derived using GFS forecasts provided every 3 h. The model topography was provided from the U.S. Geological Survey with resolutions of 10′ and 5′ for outer and inner domains, respectively. The best tracking data from the JMA was used to validate the model forecasts. The rainfall forecast was validated with 0.05° daily data of the Climate Hazards Group InfraRed Precipitation with Station (CHIRPS) product.

The NCEP provided the PREPBUFR observations and satellite radiance datasets. Satellite radiances from the AMSU-A onboard NOAA-15/16/18, the ATMS onboard NOAA-20, and the HIRS-4 onboard NOAA-18 satellite radiances were used in this study. The AMSU-A is a cross-track microwave radiometer with 30 fields of view (FOV) per scan line that scans the Earth surface within ±1089 km at nadir. It operated in the microwave frequency range of 23.8 to 89.0 GHz and was designed to capture temperature sounding information under nearly all weather conditions. The ATMS is a new microwave radiometer that used the Suomi-NPP (S-NPP) platform to provide humidity and temperature sounding. All ATMS channels were sampled every 1.11° at 96 scan positions with a cross-track scanning microwave radiometer with 22 channels, which is significantly wider than the typical 2100–2300 km for AMSU-A or MHS. As a result, ATMS data coverage shows no gaps between swaths in the tropical area [29,30]. The temperature-sounding channels of the ATMS differed significantly from those of AMUS-A in spatial sampling, FOV, and noise. However, the HIRS-4 is an atmospheric sounding instrument with multispectral data from one visible channel, as well as seven shortwave and twelve longwave infrared channels obtained from a single telescope and a rotating filter wheel containing twenty individual filters, providing the spatial resolution of approximately 10 km at nadir [31–33]. It is also a cross-track sensor, scanning every 6.4 s. It has a swath width of 2248 km to the far edge of the outer FOV centered on the subsatellite track. In this study, we used the assimilation of radiance data from the AMSU-A, ATMS, and HIRS-4 instruments onboard NOAA and Metop-B satellite platforms.

A quality control step was conducted before assimilating the satellite radiance observations to ensure that the observations assimilated into the model are reliable. Table 3 shows the characteristics of the AMSU-A, ATMS, and HIRS-4 channels. Note that channels 1–4 and 15 of AMSU-A could be contaminated by the surface due to the background temperature and emissivity being challenging to model with a high likelihood for error, the simulation of window channel radiance could be highly erratic [34]. Therefore, AMSU-A channels 10–14 were not assimilated into the model since their peaks were above the top boundary of the model. In summary, the AMSU-A channels 5–9, ATMS channels 7–14 and 19–22, and HIRS-4 channels 3–5 and 11–12 were used for the assimilation.

Table 3. AMSU-A, ATMS, and HIRS-4 channel characteristics.

Channel Number	AMSU-A Frequency (GHz)	ATMS Frequency (GHz)	HIRS-4 Frequency (GHz)
1	23.80	23.80	669
2	31.80	31.40	680
3	50.30	50.3	690
4	52.80	51.76	703
5	53.596 ± 0.115	52.8	716
6	54.40	53.596 ± 0.115	733
7	54.94	54.40	749
8	54.94	54.94	900
9	57.290	54.94	1030
10	57.290	57.290	802
11	57.290 ± 0.3222 ± 0.048	57.290	1365
12	57.290 ± 0.3222 ± 0.022	57.290 ± 0.3222 ± 0.048	1533
13	57.290 ± 0.3222 ± 0.010	57.290 ± 0.3222 ± 0.022	2188
14	57.290 ± 0.3222 ± 0.0045	57.290 ± 0.3222 ± 0.010	2210
15	89.0	57.290 ± 0.3222 ± 0.0045	2235
16		88.2	
17		165.6	
18		183.31 ± 7.0	
19		183.31 ± 4.5	
20		183.31 ± 3.0	
21		183.31 ± 1.8	
22		183.31 ± 1.0	

Unfortunately, brightness observations may differ significantly from those predicted by the WRF model. A variety of factors can contribute to biases. It was possible to calibrate systematic errors for the satellite instruments. For example, temperature and water vapor profiles used as input in the WRF model may not be as precise as they should be. In addition, the radiative transfer model was flawed and had its own limitations. As a result, before combining the satellite radiance data, any potential biases in the observations had to be addressed. In the first-guess state, the difference between the observation (O) and the first guess (B) should be free of bias. The biases in this study were addressed using variational bias correction (VarBC), a method that performs bias correction as part of the analysis by considering information from both conventional observations and the background field. The VarBC used several parameters, including scan positions between 1000–300 hPa between the 200–50 hPa layer thicknesses, the surface temperature, and the total column water vapor [35].

For bias correction during radiance assimilation, an updated bias correction coefficient was used, and this predictor was created in WRF-3DVAR. All the radiance data processing, such as quality control, bias correction, and data thinning, was conducted within the WRF-3DVAR system. The observations were assimilated into the model using a 3 h time window as a cutoff [36,37]. In the data assimilation, domain-dependent regional background error statistics were used as input.

3.4. Assimilation Methodology

The data assimilation system used in this study was the WRF model's data assimilation (WRFDA) system developed by the National Center for Atmospheric Research (NCAR) [38,39]. It has the capability of processing different types of observations. The WRFDA system is a unified model for spatial data assimilation. In this study, version 3.9.1 was used; the 3DVAR assimilation method obtained an accurate analysis of the real atmospheric state for a given time by minimizing the cost function $J(x)$ as follows:

$$J(x) = \frac{1}{2}(x - x_b)^T \boldsymbol{B}^{-1}(x - x_b) + \frac{1}{2}(y - \boldsymbol{H}(x))^T \boldsymbol{R}^{-1}(y - \boldsymbol{H}(x)), \quad (1)$$

where x is the analysis field of the atmospheric and surface variables, x_b is the background field that is usually the forecast field, y is the observation field, and $\boldsymbol{H}$ is the observation operator. $\boldsymbol{B}$ is the background error covariance matrix that was generated using the National Meteorological Center (NMC) one-month method, $\boldsymbol{R}$ is the observational and representative error covariance matrix, and $\boldsymbol{B}^{-1}$ and $\boldsymbol{R}^{-1}$ are inverse matrices of $\boldsymbol{B}$ and $\boldsymbol{R}$, respectively. The analysis field x is estimated through an iterative approach so that the solution designates a minimum variance estimate of the atmospheric state. For the direct radiance assimilation, the observation operator $\boldsymbol{H}(x)$ includes the radiative transfer model (RTM), which calculates the radiances from the model variables of x.

In the data assimilation method, due to the large dimension of $\boldsymbol{B}$, it was difficult to conduct the minimum. Generally, the matrix $\boldsymbol{B}$ is decomposed into B = UU^T, and the following preprocessing stage can be formed by decomposing Uv = $x - x_b$, where v represents the control variable, and U represents the transformation operator. One approximation is applied as:

$$y - \boldsymbol{H}(x) \approx y - H(x_b) - H(x - x_b), \tag{2}$$

where $\boldsymbol{H}$ is the linearization of the nonlinear observation operator *(H)* in the form of a first-order Taylor series expansion [40,41]. The final cost function of 3DVAR can be written as:

$$J = \frac{1}{2}V^T V + \frac{1}{2}(d - HUv)^T R^{-1}(d - HUv), \tag{3}$$

where d = $y - H(x_b)$ is the innovation.

In the experiments using radiance assimilation, a forward operator was used from Equation (1); $\boldsymbol{H}$ was used as a fast RTM to calculate the brightness temperature from the model variables in state vector x. The WRFDA has the capability to use two RTMs; these are the radiative for the TOVS RRTOV model, developed by the European Organization for the Exploitation of Meteorological Satellites (EUMETSAT) [42], and the community radiative transfer model (CRTM), developed by the US Joint Center for Satellite Data Assimilation (JCSDA) (data obtained online: ftp://ftp.emc.ncep.noaa.gov/jcsda/CRTM, accessed on 9 December 2021) [43,44]. They were also improved to support a greater number of satellite instruments that covered a broader range of the electromagnetic spectrum. The literature on the RTTOV and the CRTM discussed fast RT modeling including cloud cover. Furthermore, Scheck et al. [45] presented progress on fast RT modeling in the visible spectrum, and Eriksson et al. [46] and Geer et al. [47] published their recent microwave research. Weng et al. [48] provided a comprehensive review of radiative transfer for satellite data assimilation.

For this study, we used the CTRM as the forward operator. To simulate clear-sky radiance, the CRTM calculated the inputs of temperature and water vapor profiles in the atmosphere, surface temperature, surface wind speeds, and satellite geometry parameters. The vertical profiles of hydrometer characteristics were necessary to simulate cloud-cover radiance. The fast microwave emissivity model (FASTEM) is a two-scale emissivity model that has been utilized across ocean bodies. A different land emissivity model has been used over land in articles by Liu et al. [49] and Liu and Weng [50]. The error covariance matrix was important in the data assimilation method as it could estimate a weight between the background and observations. In the 3DVAR assimilation method, there were two different kinds of background error covariance matrices. The NMC method is used to estimate the background error covariance [51–53], known as the CV3 default option, used a global model with T170 resolution from the peak winter months to better simulate the climatology of the winter season. The control variables include the stream function ψ, the unbalanced velocity potential x_u , the unbalanced temperature T_u, the pseudo-relative humidity q, and the unbalanced surface pressure P_{su}.

4. Results and Discussions

In this section, we present the results of the Tropical Storm Dianmu forecasts from four experiments (see Table 2). The model results were compared to the JMA tracking data to assess the forecast performance. Note that the benchmark tracking data were obtained from the Japan Meteorological Agency (JMA) in Tokyo, Japan.

The forecasted tracking data of Tropical Storm Dianmu, along with the JMA's best tracking data, are presented in Figure 3. Experiments using the CNTL, RDA1, RDA2, and ALL-OBS assimilations showed a westward bias in tracking prediction compared to the JMA data. This forecast was started at 00 UTC 23 September 2021 as a 72-h forecast. During the forecasted period, the tropical storm also hit the central part of Vietnam. As shown in Figure 3, the movement of the storm was more accurately predicted with the RDA1 and ALL-OBS experiments, but storm tracking with the ALL-OBS experiment was closer to the benchmark observations at approximately 20–40 km, which was better than the average of 100–200 km. As a result of superior data coverage of the storm, the assimilations with AMSU-A, ATMS, and HIRS-4 radiance data had significant impacts on the tracking predictions. The impacts of the assimilation of radiance data on tracking forecasts were observed after 3-h, and even more so after 24-h forecast with the assimilation of the AMSU-A and ATMS observations. Significant improvements in the tracking forecasts were observed in the RDA2 experiment compared to the CNTL experiment.

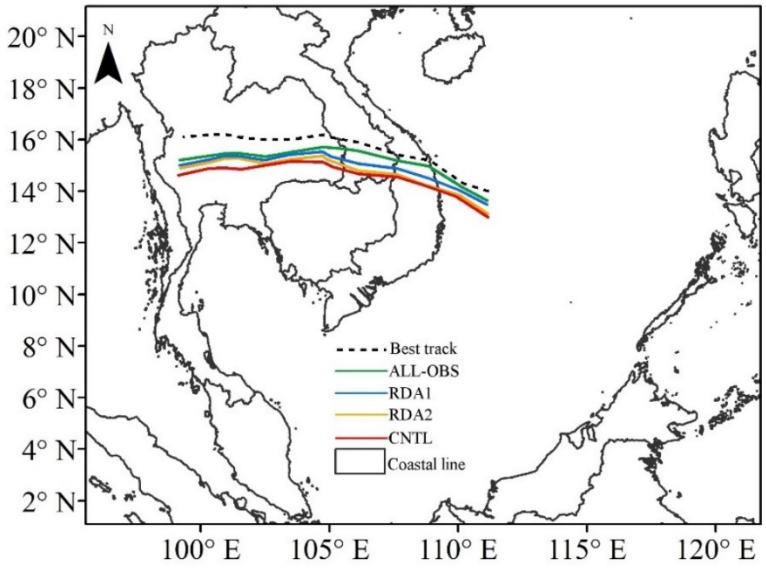

Figure 3. The model's forecasts tracks with different assimilation experiments (i.e., ALL-OBS, RDA1, RDA2, and CNTL), along with the JMA best track data (black dashed line).

The tracking errors at every 6-h interval are presented in Figure 4, which shows that the assimilated radiances were significant affected by the tracking forecasts. The results signified that the forecast tracking errors were higher in the CNTL and RDA2 experiments, as compared to the RDA1 and ALL-OBS experiments. When the deterministic forecasts were preceded by a 6-h warm start analysis, a 20-km error existed at the initial time. As shown in Figure 4, in the first 24 h, the tracking forecast in the ALL-OBS assimilation gradually grew closer to the benchmark. The tracking errors in the ALL-OBS experiment were below 40 km in the first 24 h but had a sharp increase in the last 24 h. In other words, the assimilation of the AMSU-A, ATMS, and HIRS-4 channels reduced the forecast errors, as compared to the CNTL experiment. The track of the storm was better-predicted in the ALL-OBS experiment and more obvious in the short-range forecast (up to ~24-h lead time) than the medium-range forecast, as compared to the CNTL experiment. In addition, the tracking errors of the ALL-OBS experiment were typically smaller than those in the CNTL experiment, with a maximal error of approximately 100 km.

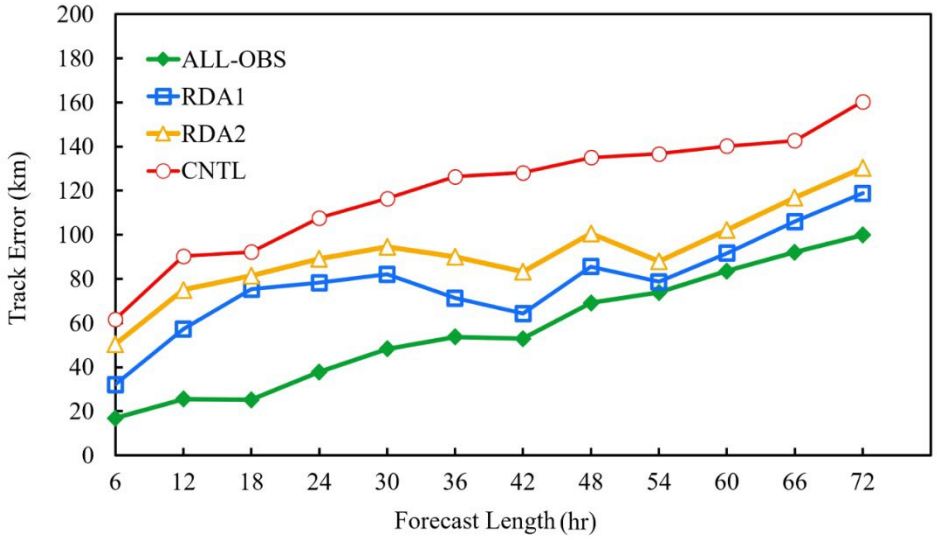

Figure 4. The tracking errors in kilometers (km) over time for the different assimilation experiments.

Figure 5 shows the time evolution of the forecasts in terms of the mean sea level pressure (MSLP) observed intensity (Figure 5a), and maximum winds (Figure 5b). The ALL-OBS experiment was found to be more accurate in forecasting the Tropical Storm Dianmu's intensification and dissipation patterns, although the JMA best tracking data were more accurate in forecasting the peak intensity of the MSLP. The forecasted storm reached its peak intensity at 18 UTC on September 23 with an MSLP of approximately 1003 hPa while the observations reported an MSLP of approximately 1004 hPa at the same time. The ALL-OBS experiment showed a similar pattern for storm intensification, although the storm dissonated 6 h earlier than in the RDA2 experiment. The CNTL experiment failed to capture the storm's dissipation, and the RDA1 and RDA2 experiments underestimated the storm's peak intensity in terms of MSLP. In these forecasts, the MSLP was closer to the best JMA tracking data in the first 24 h, as compared to the CNTL experiment; thereafter, it was underestimated. When it came to the storm's intensity, the CNTL experiment's maximum wind speed consistently underestimated the storm's rate of expansion throughout the entire forecast period. A peak wind speed of approximately 20 m/s was recorded in the ALL-OBS experiment, while the best JMA tracking data recorded a peak wind speed of approximately 18 m/s.

The wind speed (in m/s) distribution for 23 September 2021 at 00 UTC according to the NCEP FNL analysis and the different assimilation experiments are shown in Figure 6. The maximum surface winds were 20, 16, 15, and 8 m/s in the ALL-OBS, RDA1, RDA2, and CNTL experiments, respectively, and 18 m/s from FNL analysis. Winds in the region outside the storm were much weaker in the ALL-OBS experiment than in the CNTL experiment. An increase in the cyclonic wind field to 850 hPa was noted in the ALL-OBS experiment, and the wind speed increment was approximately 2–10 m/s in the region of the storm and approximately 1–3 m/s. This indicated that the ALL-OBS experiment indicated a stronger surface wind than the CNTL experiment.

Figure 7 presents the spatial distribution over 72-h of accumulated rainfall from 00 UTC on 23 September 2021 to 25 September 2021 given by the observations (CHIRPS) and from different assimilation forecasts. According to the CHIRPS, Tropical Storm Dianmu produced heavy rainfall in the north part of Vietnam, as well as two rainfalls in the west and northeastern parts of Thailand. It was slightly better-predicted in the ALL-OBS experiment than in the AMSU-A, ATMS, HIRS-4, and PREPBUFR datasets. The location of the maximum rainfall and the pattern of rainfall in the ALL-OBS experiment both agreed with the observations but were overestimated by approximately 100−150 mm regarding the magnitude of the observed rainfall in the core region of the storm. Usually, the accuracy of the forecast tracking influences the distribution of rainfall pattern. In the CNTL

experiment, we found that the rainfall was focused in an eastward direction, including higher levels of rainfall, as compared to the observed rainfall. The experiments using RDA1 and RDA2 showed that the locations of the two rainfalls in Thailand corresponded with the observations. The rainfall forecast for north Vietnam was improved, but the west and northeast Thailand rainfalls were mildly overestimated by approximately 80−120 mm. However, it was concluded that the forecasted rainfall showed that the assimilation of all the data sources (PREPBUFR, AMSU-A, ATMS, and HIRS-4) were similar to the CHIRPS rainfall data and the assimilation of the AMSU-A and ATMS radiance data enhanced the location of rainfall, as compared to the other experiments.

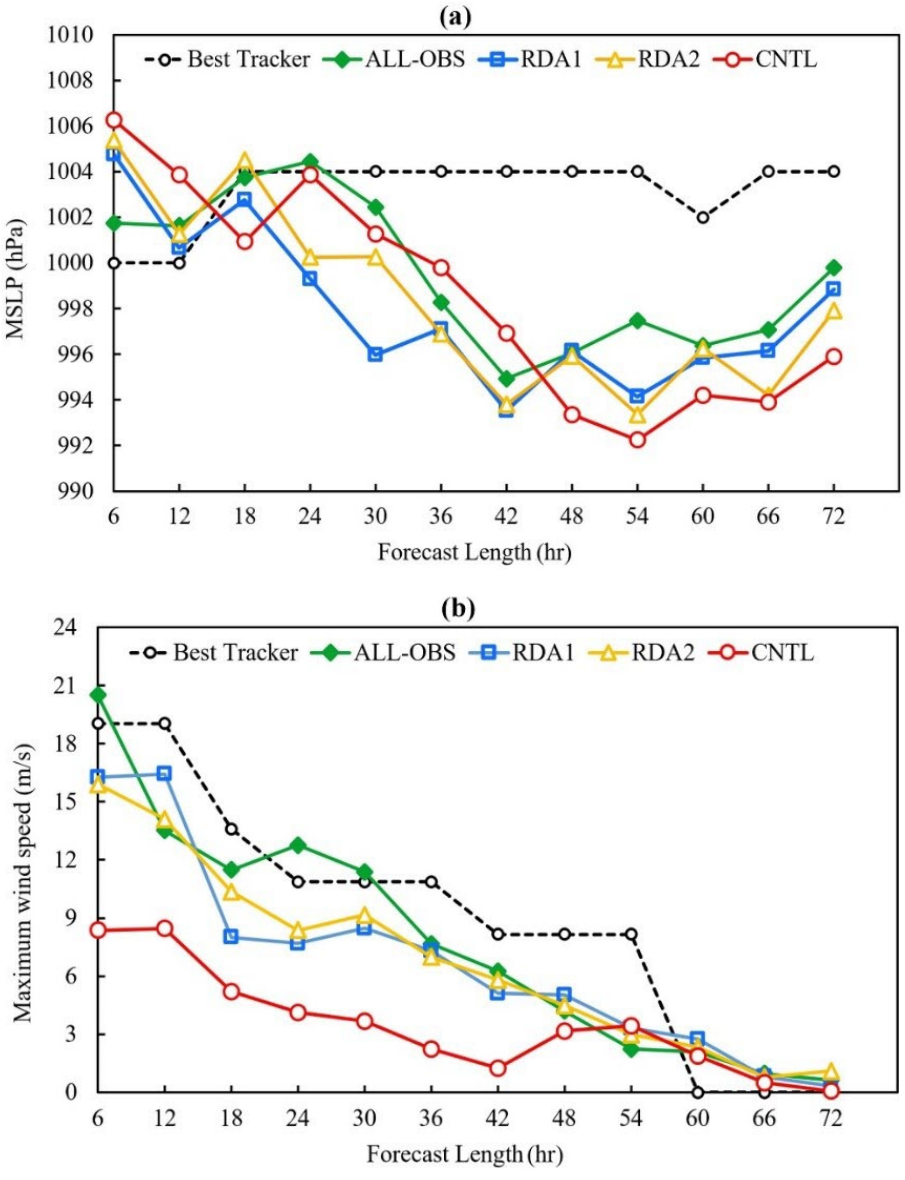

Figure 5. Variation of (**a**) mean sea level pressure (hPa) and (**b**) maximum wind (in m/s) over time (per hour) according to assimilation experiments and JMA benchmark.

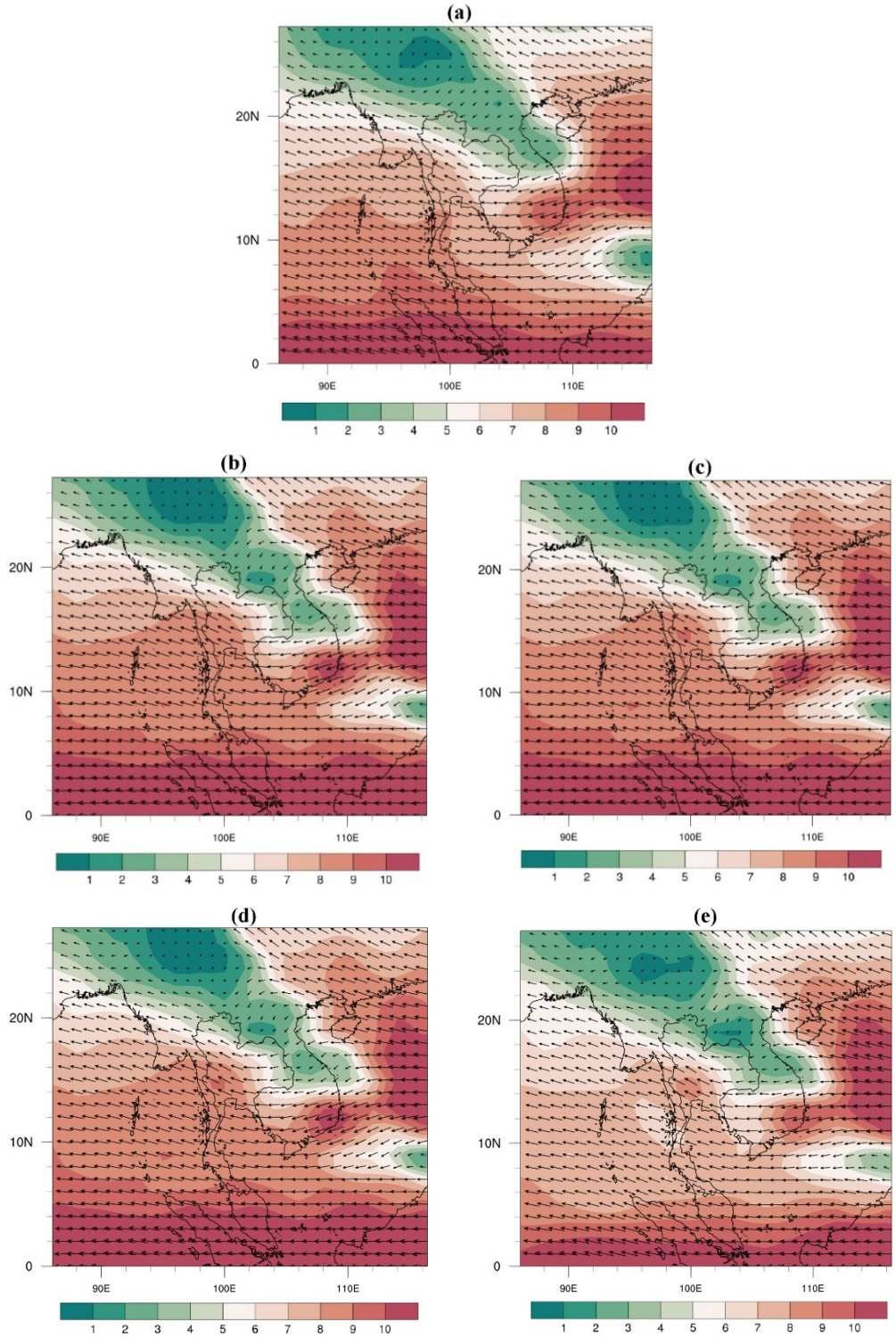

Figure 6. The 850 hPa circulation including wind field (vector, unit: m/s) at 00 UTC on 23 September 2021: (**a**) NCEP FNL analysis, (**b**) ALL-OBS, (**c**) RDA1, (**d**) RDA2, and (**e**) CNTL.

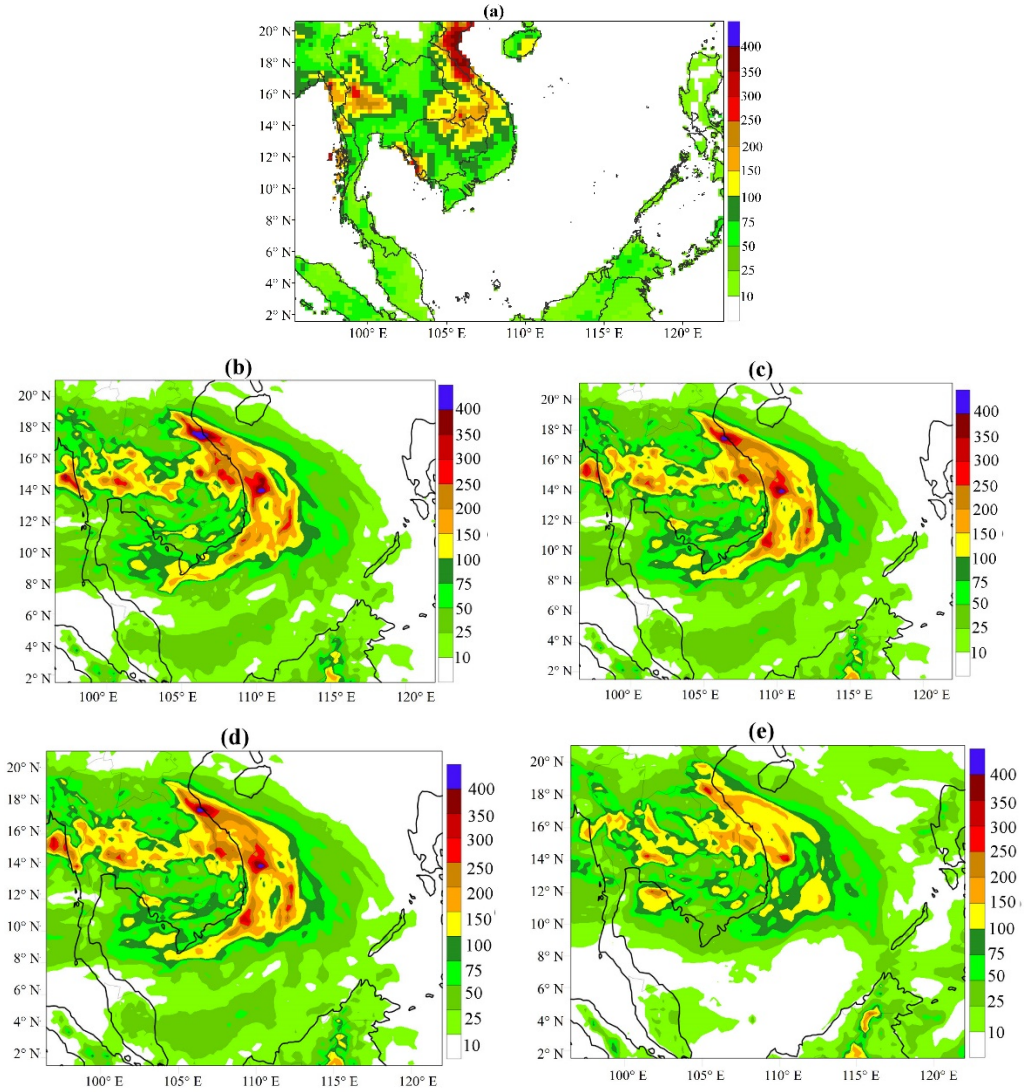

Figure 7. Spatial distribution of 72-h accumulated rainfall given by (**a**) CHIRPS analysis, (**b**) ALL-OBS, (**c**) RDA1, (**d**) RDA2, and (**e**) CNTL.

5. Conclusions

This study focused on data assimilation using a 3DVAR assimilation method for Tropical Storm Dianmu forecasts. The CNTL and radiance assimilation experiments were conducted for 72-h forecasts starting at 00 UTC on 23 September 2021. In the CNTL experiment, only the NCEP PREPBUFR datasets were assimilated. However, the AMSU-A, ATMS, and HIRS-4 satellite radiance data were also assimilated in the radiance assimilation experiments. The following conclusions were drawn according to the results of our experiments.

The assimilation of AMSU-A, ATMS, and HIRS-4 data produced a forecast with improved tracking and initial stages of the storm. The impact of the assimilation showed that the AMSU-A and ATMS radiance data provided a better forecast of storm tracking, intensity, and movements and was similar to the JMA tracking data. The trends of storm intensification and dissipation were also observed to be consistent with the RDA1 experiment. When the AMSU-A and ATMS radiance data were assimilated into the model, the storm tracking showed slight improvements. Significant improvement was found in the forecasted tracking and intensity of Tropical Storm Dianmu, providing better forecasting in the ALL-OBS experiment compared to the CNTL, RDA1, and RDA2 experiments. In addition, the 850-hPa wind fields were preferable for the maintenance of the storm. For

the 72-h accumulated rainfall forecast, the positions of the rainfalls in the ALL-OBS experiment had better agreement with the observations, whereas the rain belt in Thailand was overestimated. Finally, the tracking errors in the ALL-OBS experiment were smaller, with a maximal error of approximately 100 km, as compared to the CNTL experiment.

In the case study of Tropical Storm Dianmu, we found a positive influence from tropical storm initialization and forecasting. This was a preliminary study with AMSU-A, ATMS, and HIRS-4 satellite radiance data assimilated using a 3DVAR system. In future research, additional tropical storm events should be included to verify the effectiveness of radiance assimilation. Furthermore, more assimilation time periods should be considered for continuous improvement of the initial conditions.

Author Contributions: Conceptualization, F.W., K.T. and T.T.; methodology, validation, and writing—original draft preparation, T.T.; investigation and formal analysis, K.T. and T.T.; data curation, E.M.A.C.; writing—review and editing, F.W. and G.Y.; funding acquisition, F.W. and G.Y. All authors have read and agreed to the published version of the manuscript.

Funding: This research received no external funding. The article processing charge was funded by Beihang University.

Institutional Review Board Statement: Not applicable.

Informed Consent Statement: Not applicable.

Data Availability Statement: The NCEP Global Forecast System (GFS) analyses and forecasts data can be freely obtained online (https://rda.ucar.edu/datasets/ds084.1/, accessed on 8 April 2022). The CHIRPS datasets can be obtained online at the Climate Hazards Center (https://data.chc.ucsb.edu/products/CHIRPS-2.0/, accessed on 8 April 2022), the best track data from the JMA can be obtained online (https://www.jma.go.jp/jma/jma-eng/jma-center/rsmc-hp-pub-eg/Besttracks/bst2021.txt, accessed on 8 April 2022), and the AMSU-A, ATMS, and HIRS-4 satellite data can be obtained online (https://rda.ucar.edu/datasets/ds735.0/, accessed on 8 April 2022).

Acknowledgments: We would like to acknowledge the support of the High-Performance Computing Center at the Hydro Informatics Institute (public organization). The authors thank the availability of the NCEP Global Forecast System (GFS) Analyses and forecasts data, JMA track data, CHIRPS datasets, the AMSU-A, ATMS, and HIRS-4 satellite data.

Conflicts of Interest: The authors declare no conflict of interest.

References

1. Islam, T.; Srivastava, P.K.; Rico-Ramirez, M.A.; Dai, Q.; Gupta, M.; Singh, S.K. Tracking a tropical cyclone through WRF–ARW simulation and sensitivity of model physics. *Nat. Hazards* **2014**, *76*, 1473–1495. [CrossRef]
2. Rajeswari, J.R.; Srinivas, C.V.; Mohan, P.R.; Venkatraman, B. Impact of Boundary Layer Physics on Tropical Cyclone Simulations in the Bay of Bengal Using the WRF Model. *Pure Appl. Geophys.* **2020**, *177*, 5523–5550. [CrossRef]
3. Gray, W.M. Global view of the origin of tropical disturbances and storms. *Mon. Weather. Rev.* **1968**, *96*, 669–700. [CrossRef]
4. Sansom, H. Tropical climatology—An introduction to the climates of the low latitudes. *Earth-Sci. Rev.* **1977**, *13*, 377–378. [CrossRef]
5. Yesubabu, V.; Srinivas, C.V.; Hariprasad, K.B.R.R.; Baskaran, R. A Study on the Impact of Observation Assimilation on the Numerical Simulation of Tropical Cyclones JAL and THANE Using 3DVAR. *Pure Appl. Geophys.* **2013**, *171*, 2023–2042. [CrossRef]
6. Thodsan, T.; Wu, F.; Torsri, K.; Yang, G. Evaluation of 3DVAR Data Assimilation with Automatic Weather Station Data for Heavy Rainfall Forecasting in Thailand. In Proceedings of the 2021 IEEE International Geoscience and Remote Sensing Symposium IGARSS, Brussels, Belgium, 11–16 July 2021; pp. 7263–7266.
7. Kattamanchi, V.; Viswanadhapalli, Y.; Dasari, H.P.; Langodan, S.; Vissa, N.K.; Sanikommu, S.; Rao, S.V. Impact of assimilation of SCATSAT-1 data on coupled ocean-atmospheric simulations of tropical cyclones over Bay of Bengal. *Atmos. Res.* **2021**, *261*, 105733. [CrossRef]
8. Xu, D.; Liu, Z.; Huang, X.; Min, J.; Wang, H. Impact of assimilating IASI radiance observations on forecasts of two tropical cyclones. *Meteorol. Atmos. Phys.* **2013**, *122*, 1–18. [CrossRef]
9. Xu, D.; Min, J.; Shen, F.; Ban, J.; Chen, P. Assimilation of MWHS radiance data from the FY-3B satellite with the WRF Hybrid-3DVAR system for the forecasting of binary typhoons. *J. Adv. Model. Earth Syst.* **2016**, *8*, 1014–1028. [CrossRef]
10. Moradi, I.; Evans, K.F.; McCarty, W.; Cordero-Fuentes, M.; Gelaro, R.; Black, R.A. Assimilation of Satellite Microwave Observations over the Rainbands of Tropical Cyclones. *Mon. Weather. Rev.* **2020**, *148*, 4729–4745. [CrossRef]

11. Deb, S.; Kishtawal, C.; Kumar, P.; Kumar, A.K.; Pal, P.; Kaushik, N.; Sangar, G. Atmospheric Motion Vectors from INSAT-3D: Initial quality assessment and its impact on track forecast of cyclonic storm NANAUK. *Atmos. Res.* **2015**, *169*, 1–16. [CrossRef]
12. Singh, K.S.; Mandal, M.; Bhaskaran, P.K. Impact of radiance data assimilation on the prediction performance of cyclonic storm SIDR using WRF-3DVAR modelling system. *Arch. Meteorol. Geophys. Bioclimatol. Ser. B* **2017**, *131*, 11–28. [CrossRef]
13. Lindskog, M.; Dybbroe, A.; Randriamampianina, R. Use of Microwave Radiances from Metop-C and Fengyun-3 C/D Satellites for a Northern European Limited-area Data Assimilation System. *Adv. Atmos. Sci.* **2021**, *38*, 1415–1428. [CrossRef]
14. Xu, D.; Shu, A.; Li, H.; Shen, F.; Li, Q.; Su, H. Effects of Assimilating Clear-Sky FY-3D MWHS2 Radiance on the Numerical Simulation of Tropical Storm Ampil. *Remote Sens.* **2021**, *13*, 2873. [CrossRef]
15. Thodsan, T.; Wu, F.; Torsri, K.; Khampuenson, T.; Yang, G. Impact of the Assimilation of Multi-Platform Observations on Heavy Rainfall Forecasts in Kong-Chi Basin, Thailand. *Atmosphere* **2021**, *12*, 1497. [CrossRef]
16. Eyre, J.R.; Bell, W.; Cotton, J.; English, S.J.; Forsythe, M.; Healy, S.B.; Pavelin, E.G. Assimilation of satellite data in numerical weather prediction. Part II: Recent years. *Q. J. R. Meteorol. Soc.* **2021**, *148*, 521–556. [CrossRef]
17. Eyre, J.R.; English, S.J.; Forsythe, M. Assimilation of satellite data in numerical weather prediction. Part I: The early years. *Q. J. R. Meteorol. Soc.* **2019**, *146*, 49–68. [CrossRef]
18. Tian, X.; Zou, X. Capturing Size and Intensity Changes of Hurricanes Irma and Maria (2017) from Polar-Orbiting Satellite Microwave Radiometers. *J. Atmos. Sci.* **2018**, *75*, 2509–2522. [CrossRef]
19. Seto, R.; Koike, T.; Rasmy, M. Heavy rainfall prediction applying satellite-based cloud data assimilation over land. *J. Geophys. Res. Atmos.* **2016**, *121*, 9737–9755. [CrossRef]
20. Phunthirawuthi, P.; Wu, F.; Boonyuen, P. Performance analysis of GPS Radio Occultation assimilation for tropical cyclone monitoring. In Proceedings of the 2016 IEEE International Geoscience and Remote Sensing Symposium (IGARSS), Beijing, China, 10–15 July 2016; pp. 2181–2184.
21. Chandrasekar, R.; Balaji, C. Impact of physics parameterization and 3DVAR data assimilation on prediction of tropical cyclones in the Bay of Bengal region. *Nat. Hazards* **2015**, *80*, 223–247. [CrossRef]
22. Chandrasekar, R.; Sahu, R.K.; Balaji, C. Assimilation of multi-channel radiances in mesoscale models with an ensemble technique to improve track forecasts of Tropical cyclones. *J. Earth Syst. Sci.* **2022**, *131*, 83. [CrossRef]
23. Sentinel Asia. Tropical Storm Dianmu Flood in Thailand on 1 October 2021. Available online: https://sentinel-asia.org/EO/2021/article20211001TH.html (accessed on 1 February 2022).
24. Rogers, E.; Black, T.L.; Deaven, D.G.; Dimego, G.J.; Zhao, Q.; Baldwin, M.E.; Junker, N.W.; Lin, Y. Changes to the Operational "Early" Eta Analysis/Forecast System at the National Centers for Environmental Prediction. *Weather Forecast.* **1996**, *11*, 391–413. [CrossRef]
25. Hong, S.-Y.; Noh, Y.; Dudhia, J. A New Vertical Diffusion Package with an Explicit Treatment of Entrainment Processes. *Mon. Weather Rev.* **2006**, *134*, 2318–2341. [CrossRef]
26. Iacono, M.J.; Delamere, J.S.; Mlawer, E.J.; Shephard, M.W.; Clough, S.A.; Collins, W.D. Radiative Torcing by long-lived Greenhouse Gases: Calculations with the AER Radiative Transfer Models. *J. Geophys. Res.* **2008**, *113*, D13. [CrossRef]
27. Dudhia, J. Numerical Study of Convection Observed during the Winter Monsoon Experiment Using a Mesoscale Two-Dimensional Model. *J. Atmos. Sci.* **1989**, *46*, 3077–3107. [CrossRef]
28. Janjic, Z.I. The Step-Mountain Eta Coordinate Model: Further Developments of the Convection, Viscous Sublayer, and Turbulence Closure Schemes. *Mon. Weather Rev.* **1994**, *122*, 927–945. [CrossRef]
29. Kim, E.J.; Leslie, V.; Lyu, J.; Smith, C.K.; McCormick, L.; Anderson, K. Pre-Launch Characterization of the Advanced Technology Microwave Sounder (ATMS) on the Joint Polar Satellite System-1 Satellite (JPSS-1). In Proceedings of the EGU General Assembly, Vienna, Austria, 17–22 April 2016.
30. Kim, E.J.; Leslie, R.V.; Lyu, C.-H.J.; Smith, C.K.; Osaretin, I.; Abraham, S.; Sammons, M.; Anderson, K.; Amato, J.; Fuentes, J.; et al. Pre-Launch Performance of the Advanced Technology Microwave Sounder (ATMS) on the Joint Polar Satellite System-2 Satellite (JPSS-2). In Proceedings of the IGARSS 2020-2020 IEEE International Geoscience and Remote Sensing Symposium, Waikoloa, HI, USA, 26 September–2 October; pp. 6353–6356.
31. You, Q.; Min, J.; Kang, S.; Pepin, N. Poleward expansion of the tropical belt derived from upper tropospheric water vapour. *Int. J. Clim.* **2014**, *35*, 2237–2242. [CrossRef]
32. ESA. HIRS/4 Performance. Available online: https://www.esa.int/Applications/Observing_the_Earth/Meteorological_missions/MetOp/About_HIRS_4 (accessed on 3 February 2022).
33. Cao, C.; Xu, H.; Sullivan, J.; McMillin, L.M.; Ciren, P.; Hou, Y.-T. Intersatellite Radiance Biases for the High-Resolution Infrared Radiation Sounders (HIRS) on board NOAA-15, -16, and -17 from Simultaneous Nadir Observations. *J. Atmos. Ocean. Technol.* **2005**, *22*, 381–395. [CrossRef]
34. Baker, N.L.; Hogan, T.F.; Campbell, W.F.; Pauley, R.L.; Swadley, S.D. *The Impact of AMSU-A Radiance Assimilation in the U.S. Navy's Operational Global Atmospheric Prediction System (NOGAPS)*; Atmospheric Dynamics and Prediction Branch, Marine Meteorology Division: Monterey, CA, USA, 2005.
35. Auligné, T.; McNally, A.P.; Dee, D.P. Adaptive bias correction for satellite data in a numerical weather prediction system. Q. *J. R. Meteorol. Soc.* **2007**, *133*, 631–642. [CrossRef]
36. Poterjoy, J.; Zhang, F. Intercomparison and Coupling of Ensemble and Four-Dimensional Variational Data Assimilation Methods for the Analysis and Forecasting of Hurricane Karl (2010). *Mon. Weather Rev.* **2014**, *142*, 3347–3364. [CrossRef]

37. Greeshma, M.M.; Srinivas, C.V.; Yesubabu, V.; Naidu, C.V.; Baskaran, R.; Venkatraman, B. Impact of local data assimilation on tropical cyclone predictions over the Bay of Bengal using the ARW model. *Ann. Geophys.* **2015**, *33*, 805–828. [CrossRef]
38. Barker, D.; Huang, X.-Y.; Liu, Z.; Auligné, T.; Zhang, X.; Rugg, S.; Ajjaji, R.; Bourgeois, A.; Bray, J.; Chen, Y.; et al. The Weather Research and Forecasting Model's Community Variational/Ensemble Data Assimilation System: WRFDA. *Bull. Am. Meteorol. Soc.* **2012**, *93*, 831–843. [CrossRef]
39. Ide, K.; Courtier, P.; Ghil, M.; Lorenc, A.C. Unified Notation for Data Assimilation: Operational, Sequential and Variational. *J. Meteorol. Soc. Jpn.* **1997**, *75*, 181–189. [CrossRef]
40. Tarantola, A.; Valette, B. Generalized Nonlinear Inverse Problems Solved Using the Least Squares Criterion. *Rev. Geophys.* **1982**, *20*, 219–232. [CrossRef]
41. Sugimoto, S.; Crook, N.A.; Sun, J.; Xiao, Q.; Barker, D.M. An Examination of WRF 3DVAR Radar Data Assimilation on Its Capability in Retrieving Unobserved Variables and Forecasting Precipitation through Observing System Simulation Experiments. *Mon. Weather. Rev.* **2009**, *137*, 4011–4029. [CrossRef]
42. Saunders, R.; Hocking, J.; Turner, E.; Rayer, P.; Rundle, D.; Brunel, P.; Vidot, J.; Roquet, P.; Matricardi, M.; Geer, A.; et al. An update on the RTTOV fast radiative transfer model (currently at version 12). *Geosci. Model Dev.* **2018**, *11*, 2717–2737. [CrossRef]
43. Han, Y.; Weng, F.; Liu, Q.; Van Delst, P. A fast radiative transfer model for SSMIS upper atmosphere sounding channels. *J. Geophys. Res. Earth Surf.* **2007**, *112*, D11. [CrossRef]
44. Weng, F. Advances in Radiative Transfer Modeling in Support of Satellite Data Assimilation. *J. Atmos. Sci.* **2007**, *64*, 3799–3807. [CrossRef]
45. Scheck, L.; Frèrebeau, P.; Buras-Schnell, R.; Mayer, B. A fast radiative transfer method for the simulation of visible satellite imagery. *J. Quant. Spectrosc. Radiat. Transf.* **2016**, *175*, 54–67. [CrossRef]
46. Eriksson, P.; Ekelund, R.; Mendrok, J.; Brath, M.; Lemke, O.; Buehler, S.A. A general database of hydrometeor single scattering properties at microwave and sub-millimetre wavelengths. *Earth Syst. Sci. Data* **2018**, *10*, 1301–1326. [CrossRef]
47. Geer, A.J. Physical characteristics of frozen hydrometeors inferred with parameter estimation. Atmospheric Meas. *Atmos. Meas. Tech.* **2021**, *14*, 5369–5395. [CrossRef]
48. Weng, F.; Johnson, B.T.; Zhang, P.; English, S. Preface for the special issue of radiative transfer models for satellite data assimilation. *J. Quant. Spectrosc. Radiat. Transf.* **2020**, *244*, 106826. [CrossRef]
49. Liu, Q.; Xue, Y.; Li, C. Sensor-based clear and cloud radiance calculations in the community radiative transfer model. *Appl. Opt.* **2013**, *52*, 4981–4990. [CrossRef] [PubMed]
50. Liu, Q.; Weng, F. Using Advanced Matrix Operator (AMOM) in Community Radiative Transfer Model. *IEEE J. Sel. Top. Appl. Earth Obs. Remote Sens.* **2013**, *6*, 1211–1218. [CrossRef]
51. Wu, W.-S.; Purser, R.J.; Parrish, D.F. Three-Dimensional Variational Analysis with Spatially Inhomogeneous Covariances. *Mon. Weather Rev.* **2002**, *130*, 2905–2916. [CrossRef]
52. Purser, R.J.; Wu, W.; Parrish, D.F.; Roberts, N.M. Numerical Aspects of the Application of Recursive Filters to Variational Statistical Analysis. Part II: Spatially Inhomogeneous and Anisotropic General Covariances. *Mon. Weather Rev.* **2003**, *131*, 1524–1535. [CrossRef]
53. Wang, H.; Huang, X.-Y.; Sun, J.; Xu, D.; Zhang, M.; Fan, S.; Zhong, J. Inhomogeneous Background Error Modeling for WRF-Var Using the NMC Method. *J. Appl. Meteorol. Clim.* **2014**, *53*, 2287–2309. [CrossRef]